Few-Body Bound States of Dipole-Dipole Interacting Rydberg Atoms

Martin Kiffner[1,2], Mingxia Huo[1,2], Wenhui Li[1,3], and Dieter Jaksch[2,1]
Centre for Quantum Technologies, National University of Singapore, 3 Science Drive 2, Singapore 117543[1]
Clarendon Laboratory, University of Oxford, Parks Road, Oxford OX1 3PU, United Kingdom[2] *and*
Department of Physics, National University of Singapore, 117542, Singapore[3]

We show that the resonant dipole-dipole interaction can give rise to bound states between two and three Rydberg atoms with non-overlapping electron clouds. The dimer and trimer states arise from avoided level crossings between states converging to different fine structure manifolds in the limit of separated atoms. We analyze the angular dependence of the potential wells, characterize the quantum dynamics in these potentials and discuss methods for their production and detection. Typical distances between the atoms are of the order of several micrometers which can be resolved in state-of-the-art experiments. The potential depths and typical oscillation frequencies are about one order of magnitude larger as compared to the dimer and trimer states investigated in [PRA **86** 031401(R) (2012)] and [PRL **111** 233003 (2014)], respectively. We find that the dimer and trimer molecules can be aligned with respect to the axis of a weak electric field.

PACS numbers: ,31.50.-x,32.80.Ee,82.20.Rp

arXiv:1404.3825v2 [physics.atom-ph] 8 Jul 2014

I. INTRODUCTION

Rydberg atoms [1] are atoms where at least one electron is in a highly excited state. State-of-the-art experiments offer unprecedented control over the position of cold and ultracold Rydberg atoms and allow one to prepare them in specific internal quantum states. These features combined with the exaggerated properties of Rydberg atoms make them ideally suited for investigating the quantum physics of few-body interactions. For example, the interaction of a single Rydberg electron with ground state atoms was investigated in [2–8]. More specifically, a single ground state atom interacting with a Rydberg electron gives rise to so-called trilobite molecules [2, 3] that are several orders of magnitude larger than conventional molecules. In addition, these molecules can possess giant permanent electric dipole moments [4, 5] and can be aligned by external magnetic fields [8]. It was shown that the interaction of one Rydberg electron with two ground state atoms can give rise to trimer states [6], and the interaction of a single Rydberg electron with a Bose-Einstein condensate was investigated in [7].

A second example is given by the theoretically well-understood and tunable dipole-dipole (DD) interaction. Recently, the direct measurement of the van der Waals interaction between two Rydberg atoms was achieved [9], and excellent agreement between theory and experiment was found. The DD interaction between Rydberg atoms is at the heart of various exceptional phenomena in quantum optics [10] and quantum information science [11]. Examples are given by the Rydberg blockade effect [12–15], the realization of quantum gates and entanglement [16, 17] and DD-induced artificial gauge fields acting on the relative motion of two Rydberg atoms were predicted in [18–20]. Moreover, several schemes have been developed where the DD interaction between Rydberg atoms with non-overlapping electron clouds gives rise to giant molecules [21–29]. Interatomic spacings in these so-called macrodimers typically exceed $1\,\mu$m and thus their positions become experimentally resolvable [30, 31]. The binding mechanism of the macrodimer scheme proposed in [23] and observed in [24] can be explained in terms of avoided crossings between Stark shifted states converging to van der Waals shifted two-atom states for large atomic separations. On the contrary, the dimer and trimer states in [28, 29] arise from avoided crossings between Stark shifted states within a small manifold of near-resonantly coupled states. The resonant character of the DD interaction between those states reduces the number of relevant atomic levels. This feature leads to insightful and transparent physics and allows one to account for the anisotropic nature of DD induced trapping potentials in the presence of external electric fields.

Here we investigate bound dimer and trimer states in DD interacting Rydberg atoms based on the Rydberg level scheme shown in Fig. 1(a). This level scheme is an extension of the Rydberg macrodimer proposal in [28] because it contains the $np_{1/2}$ states in addition to the $np_{3/2}$ states. The purpose of the present work is twofold. First, we investigate the influence of the $np_{1/2}$ states on previous results [28, 29] and show that the qualitative results remain unchanged. Second, we find that the presence of the $np_{1/2}$ states gives rise to a novel type of dimer and trimer states. These states are more deeply bound than the states reported in [28, 29] and do not require an external electric field. They can be explained in terms of avoided crossings between Rydberg states that are separated by the fine structure interval in the non-interacting limit of large atomic separations. We show that the dimer and trimer states arising from the presence of the $np_{1/2}$ states can be efficiently excited via microwave fields and find that the quantum dynamics in these wells is at least one order of magnitude faster as compared to previous results [28, 29]. A weak electric field breaks the spherical symmetry of the system and allows one to align the dimer and trimer configurations with respect to the field axis.

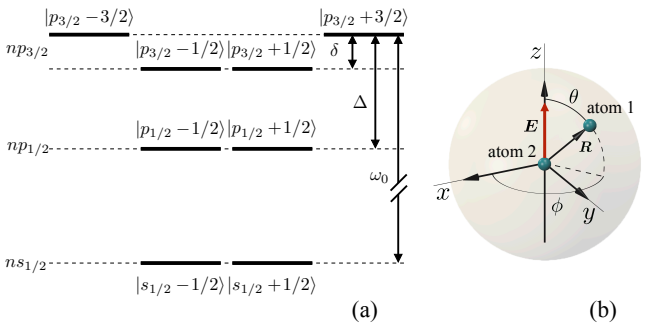

FIG. 1. (Color online) (a) Level structure of a single Rydberg atom including the $ns_{1/2}$, $np_{1/2}$ and $np_{3/2}$ Zeeman manifolds. The fine structure interval Δ and the Stark splitting δ are defined as $\hbar\Delta = E_{p_{1/2}\pm1/2} - E_{p_{3/2}\pm3/2} < 0$ and $\hbar\delta = E_{p_{3/2}\pm1/2} - E_{p_{3/2}\pm3/2} < 0$, respectively. Note that both parameters Δ and δ are negative. (b) Two DD interacting atoms with relative position $\boldsymbol{R}$. An electric field $\boldsymbol{E}$ is applied along the z direction.

This paper is organized as follows. We focus on two-atom bound states in Sec. II and discuss novel dimer states arising from the inclusion of the $np_{1/2}$ states. We identify the physical origin of the binding mechanism and investigate the influence of the $np_{1/2}$ states on the bound states reported in [28]. In Sec. III we analyze three-atom bound states induced by the mechanism explained in Sec. II and study the impact of the $np_{1/2}$ states on the trimer potential wells reported in [29]. The conclusion of our work is presented in Sec. IV.

II. TWO-ATOM BOUND STATES

We investigate two-atom bound states generated by the DD interaction for Rydberg atoms with the internal level structure shown in Fig. 1(a) and placed into an external electric field $\boldsymbol{E}$. Deeply bound molecular states arise because of the inclusion of the $np_{1/2}$ manifold. Their size is determined by the length scale r_0 which is the distance between two Rydberg atoms where the DD interaction equals the fine structure interval $\hbar|\Delta|$. The effect of the $np_{1/2}$ states on the bound dimer states investigated in [28], which appear at larger atomic distances R_0 where $\hbar|\delta|$ equals the strength of the DD interaction, is negligible.

In Sec. II A we describe the two-atom interacting system and define the relevant length and energy scales. This is followed by a qualitative discussion of the binding mechanism in Sec. II B. In Sec. II C we discuss the properties of the potential surfaces leading to bound molecular states and the quantum dynamics of the relative atomic motion in these potentials. We conclude the section by describing possible methods for preparing and detecting the bound molecular states.

A. The system

We first consider a single alkali atom with Rydberg energy level structure $|l_j m\rangle$ and principal quantum number $n \gg 1$ as shown in Fig. 1(a). In our standard notation l labels the orbital angular momentum of the Rydberg excited valence electron and j its total angular momentum. The projection of the electron's angular momentum onto the z-axis is denoted by m. The levels $|s_{1/2} \pm 1/2\rangle$ are separated from the $|p_{3/2} \pm 3/2\rangle$ levels by energy $\hbar\omega_0$. An external electric field $\boldsymbol{E}$ along the z-direction induces a Stark shift δ between states $|p_{3/2} \pm 1/2\rangle$ and $|p_{3/2} \pm 3/2\rangle$. So far this level structure is identical to that considered in [28, 29]. In contrast to this previous work we here also include the $np_{1/2}$ states into our considerations. These are separated from the $np_{3/2}$ states by the fine structure splitting Δ which will typically be much larger than the electric field induced Stark shift δ. Specifically, in our calculations we will assume $\Delta/\delta = 100$. This choice corresponds to weak electric fields of the order of 1 V/cm [29] such that the mixing of states with opposite parity is negligible [28]. For Rubidium atoms with $n \geq 30$ we find [32] $\omega_0 \approx 40\,|\Delta|$, and thus the energy $\hbar\omega_0$ of the $ns - np$ interval is much larger than any energies of interest in this work. The internal atomic Rydberg levels in Fig. 1(a) are described by the Hamiltonian $H_{\rm A}$ whose explicit form is given in Appendix A.

The Hamiltonian describing the relative motion and internal degrees of freedom of two DD interacting atoms is given by

$$H = \frac{\hat{\boldsymbol{p}}^2}{2\mu} + H_{\rm int}. \tag{1}$$

Here $\hat{\boldsymbol{p}}$ is the relative momentum operator canonically conjugate to the distance operator between the atoms $\hat{\boldsymbol{R}}$. The reduced mass of the two-atom system is denoted by μ. The second term $H_{\rm int}$ describes the internal dynamics of the two atoms and can be expressed as

$$H_{\rm int} = \sum_{\alpha=1}^{2} H_{\rm A}^{(\alpha)} + V_{12}(\hat{\boldsymbol{R}}), \tag{2}$$

where $H_{\rm A}^{(\alpha)}$ describes the energy levels of atom α and $V_{12}(\boldsymbol{R})$ is the DD interaction between the two atoms at separation $\boldsymbol{R}$ as detailed in Appendix A. Note the lack of an external trapping potential for the Rydberg energy levels.

In this work we use the Born-Oppenheimer approximation to obtain the adiabatic energy surfaces for the relative atomic motion. Following the approach in [28] we diagonalize the Hamiltonian $H_{\rm int}$ replacing $\hat{\boldsymbol{R}} \to \boldsymbol{R}$. This calculation (for details see Appendix A) yields eigenstates of the internal degrees of freedom which parametrically depend on the interatomic separation $\boldsymbol{R}$. For all potential surfaces describing bound states we have verified via semi-classical calculations [29] that the atomic motion on potential wells remains adiabatic and hence

this approximation is justified. The reason is that the potential surfaces describing bound states are energetically well separated from other curves, and the considered velocity of the cold atoms in the wells is sufficiently small.

Before quantitatively investigating these energy surfaces we describe the physical mechanism that leads to potential minima and hence bound molecular states of the two atoms. The length scale at which these bound states occur is determined by the distance r_0 between the atoms where the DD interaction strength equals the energy separation between the $np_{3/2}$ and the $np_{1/2}$ levels. As shown in Appendix A this value is given by

$$r_0 = \left[\frac{|\mathcal{D}|^2}{4\pi\varepsilon_0\hbar|\Delta|}\right]^{1/3}, \tag{3}$$

where $\mathcal{D}$ is a reduced dipole matrix element defined in Appendix A and ε_0 is the dielectric constant. We note that this definition is different from R_0 in previous work [28] where the characteristic molecule size was determined by δ instead of Δ. While Δ will typically be two orders of magnitude larger than δ the value of r_0 reduces only with the cube root of this frequency ratio hence still giving molecules with sizes on the order of microns. For instance, in the case of Rb atoms with $n = 40$, the splitting is $\Delta \simeq 2\pi \times 1$GHz, which yields $r_0 \approx 1\mu$m.

B. Binding mechanism

In this section we provide a simple explanation for the formation of bound states in DD interacting Rydberg atoms. We describe the physical mechanism by means of the two-atom system shown in Fig. 1, but the general idea does also apply to the dimer and trimer states investigated in [28] and [29], respectively.

We consider the subspace of $nsnp$ states that are directly coupled via the DD interaction. In order to describe the general level structure of DD-coupled two-atom states we ignore the Zeeman sublevels and any Stark shifts between them. In this case, each atom reduces to a three-level system with states $|s_{1/2}\rangle$, $|p_{1/2}\rangle$ and $|p_{3/2}\rangle$. The fine structure splitting Δ gives rise to two different energy asymptotes for large values of R. They correspond to the $ns_{1/2}np_{3/2}$ and $ns_{1/2}np_{1/2}$ manifolds differing in energy by $\hbar|\Delta|$ for $R \to \infty$, see Fig. 2(a). The $ns_{1/2}np_{3/2}$ manifold consists of the states $|s_{1/2}, p_{3/2}\rangle$ and $|p_{3/2}, s_{1/2}\rangle$ that are resonantly coupled by the DD interaction. Diagonalization of the DD interaction within the $ns_{1/2}np_{3/2}$ manifold leads to the potential curves shown by the black solid and red dot-dashed lines in Fig. 2(a). The energy splitting between them scales as $1/R^3$. An equivalent analysis applies to $ns_{1/2}np_{1/2}$ manifold comprising the states $|s_{1/2}, p_{1/2}\rangle$ and $|p_{1/2}, s_{1/2}\rangle$. The DD interaction between them results in position-dependent energies that are shown by the blue dashed and green dotted lines in Fig. 2(a).

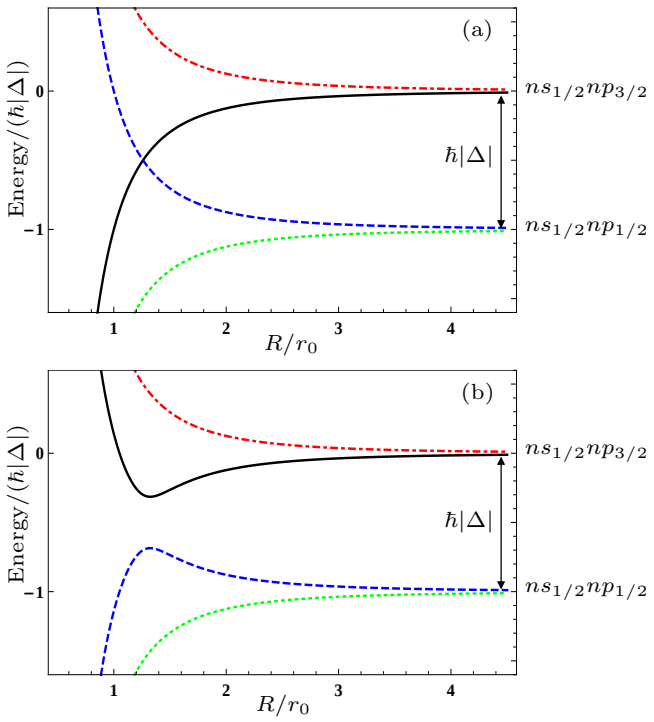

FIG. 2. (Color online) Simplified level structure of the DD coupled $nsnp$ states ignoring all Zeeman sublevels of the level scheme in Fig. 1(a). (a) Position-dependent energies within the $ns_{1/2}np_{3/2}$ ($ns_{1/2}np_{1/2}$) manifold are shown by the black solid and red dot-dashed (blue dashed and green dotted) lines. The cross-coupling Ω_{cc} in Eq. (4) between different manifolds is assumed to be zero. (b) Same as in (a) but with $\Omega_{cc} \neq 0$ resulting in an avoided level crossing between the black solid and blue dashed lines.

So far we have ignored the DD coupling between states belonging to different manifolds. This is the reason why the blue dashed and black solid lines in Fig. 2(a) cross. In general, the DD interaction will couple states in the $ns_{1/2}np_{3/2}$ manifold with those in $ns_{1/2}np_{1/2}$, i.e.,

$$\Omega_{cc} = |\langle s_{1/2}, p_{3/2}|V_{12}|p_{1/2}, s_{1/2}\rangle| \neq 0. \tag{4}$$

The DD coupling between the blue dashed and black solid lines in Fig. 2(b) is van der Waals like for large separations $R \gg r_0$ and turns into a resonant DD interaction near $R \approx r_0$, where the characteristic length scale r_0 is defined in Eq. (3). Most importantly, a non-zero cross-coupling Ω_{cc} results in an avoided level crossing between the black solid and blue dashed curves giving rise to a potential minimum, see Fig. 2(b).

In the following section II C we investigate the level structure of the DD coupled $nsnp$ states taking into account the full level scheme shown in Fig. 1(a).

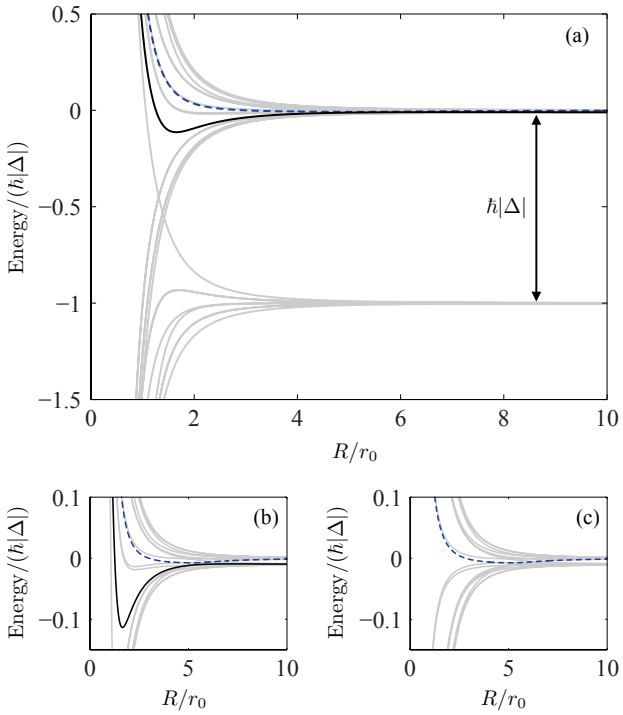

FIG. 3. (Color online) (a) All potential curves in the $nsnp$ manifold. The black solid line shows the deepest trapping potential and the blue dashed line corresponds to the dimer state investigated in [28]. (b) Magnified view of potential curves converging to the $ns_{1/2}np_{3/2}$ asymptote. Note the changed energy scale as compared to (a). (c) All states in the nsnp manifold but without the $np_{1/2}$ states as in [28]. In (a)-(c), the parameters are $\Delta/\delta = 100$ and $\theta = \pi/2$.

C. Potential surfaces

We consider the subspace of $nsnp$ states that are near-resonantly coupled by the DD interaction. Other two-atom states cause a negligible van der Waals shift for $R \geq r_0$ if their energy separation from the $nsnp$ manifold is large as compared to $\hbar|\Delta|$. Note that such a clear separation between resonantly and off-resonantly coupled states is not possible in other schemes [21–27] which are based on a large manifold of van der Waals coupled states. In Fig. 3(a) we plot the $nsnp$ eigenstates as a function of atomic distance R and angle $\theta = \pi/2$. For large distances the manifolds of $ns_{1/2}np_{1/2}$ and $ns_{1/2}np_{3/2}$ states are seen to be separated by energy $\hbar|\Delta|$. As described above when the DD interaction becomes comparable to this energy at around r_0 it leads to avoided crossings between curves of the two manifolds giving rise to potential wells. The deepest well with a minimum near $R_p \approx 1.7r_0$ is shown as a black solid line in Fig. 3(a). The well depth is approximately given by $0.1\hbar|\Delta|$ corresponding to trapping frequencies of the order of 100 MHz for $n \approx 40$. Note that the influence of the Stark shift $|\delta| \ll |\Delta|$ on this potential well is small. More details and the molecular states bound by this potential well will be analyzed in II C 1.

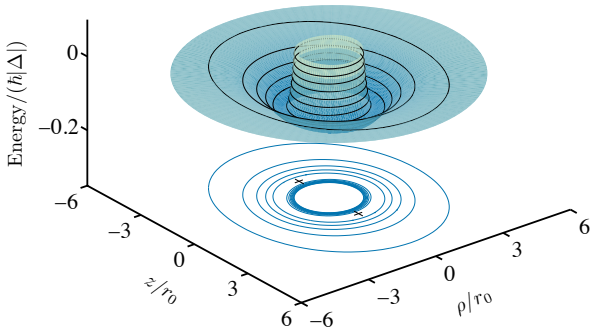

FIG. 4. (Color online) The potential well indicated by the black solid line in Fig. 3(a) in the $\rho - z$ plane for $\Delta/\delta = 100$. The two absolute minima of the potential well along the z axis are indicated by crosses in the contour projection of the potential.

In Fig. 3(b) we show a magnified view of the region investigated in [28]. This is compared to the potential curve first described there which is plotted in Fig. 3(c) ignoring the $ns_{1/2}np_{1/2}$ manifold. The minimum of the potential is located at approximately $R_0 = 100^{1/3}r_0 \approx 4.6r_0$ where the DD coupling between the $ns_{1/2}np_{1/2}$ and $ns_{1/2}np_{3/2}$ manifolds is negligible as confirmed by comparison with Fig. 3(b). We find that in the vicinity of R_0 the shape of the potential well, and hence the properties of the corresponding molecular states, are nearly unchanged by the presence of $np_{1/2}$ states. Only for smaller separations we obtain a noticeable change of the curve which, however, does not affect the properties of bound states discussed in [28].

1. *Quantum dynamics*

In Fig. 4 we show the energy surface of the deeply bound molecular potential of Fig. 3(a) as a function of $\rho = \sqrt{x^2 + y^2}$ and z. Due to the electric field in z direction and the associated Stark shift the potential well is not isotropic but the azimuthal symmetry is preserved. Since $|\delta| \ll |\Delta|$ the asymmetry of the potential well in Fig. 4 is not very pronounced. However, there are two absolute minima along the z axis at $R_p \approx 1.7r_0$. This allows one to align the molecule in the direction of the electric field. Expanding the potential around one of its minima to second order and diagonalizing the resulting Hessian matrix [29] we obtain the vibrational frequencies of the molecular motion $\omega_1 = \omega_2 \approx 0.07\omega_{\rm vib}$ and $\omega_3 \approx 0.80\omega_{\rm vib}$ where

$$\omega_{\rm vib} = \sqrt{\frac{\hbar|\Delta|}{\mu r_0^2}}. \tag{5}$$

The typical vibrational frequency is about $100^{5/6} \approx 46.4$ larger than the corresponding frequency in [28, 29] where the characteristic energy scale was given by the Stark shift δ instead of Δ. It follows that the quantum dynamics in the new dimer states is roughly one order of magnitude faster. For $\delta = 0$ the potential surfaces become isotropic and only one vibrational mode remains. The two other modes are rotational with $E_{\rm rot} = \ell(\ell+1)\hbar^2/2I$, where ℓ is the non-negative integer rotational quantum number and $I \simeq \mu r_0^2$ denotes the typical moment of inertia.

The lifetime of the molecules is limited by the lifetime of Rydberg atoms due to spontaneous decay [28]. At a temperature of 300μK we estimate a decay rate of approximately 25kHz for Rydberg states in ^{85}Rb with $n = 40$ [33]. For the same parameters we find $\omega_1 = \omega_2 \approx 2\pi \times 36$kHz, $\omega_3 \approx 2\pi \times 419$kHz and $\hbar/I \approx 2\pi \times 0.1$ kHz indicating that molecular vibrations can be resolved within the life time of the molecules while rotational excitations will not be observable. The equilibrium distance between the atoms for $n = 40$ is given by $R_p \approx 1.7\mu$m. This value increases to $R_p \approx 4.0\mu$m for $n = 60$ which is experimentally attainable [9, 30, 31].

2. *Preparation and detection*

Recent experimental progress has enabled the trapping of individual ultracold atoms separated by a controllable distance on the order of r_0 using microscopic optical traps [9]. We may hence assume the preparation of Rydberg molecules to start from two ground state atoms separated by the size of the targeted Rydberg molecule state $|\psi_p\rangle$. A two-photon excitation [34–36] as schematically shown in Fig. 5(a) can then be used to promote the atoms from the ground state manifold $|gg\rangle$ via an intermediate optically excited state $|ee\rangle$ to the state

$$|\psi_i\rangle = |s_{1/2} + 1/2, s_{1/2} + 1/2\rangle \tag{6}$$

in the $nsns$ manifold. The atoms in the $nsns$ manifold only weakly interact via the van der Waals interaction leading to a blockade radius much smaller than their separation. Also, atoms excited to a Rydberg state will no longer be trapped by the optical potential [9]. This is followed by a microwave excitation, also shown in Fig. 5(a), to $|\psi_p\rangle$ in the $nsnp$ manifold which is bound solely by the DD interaction.

For left-circularly polarized light $\vec{\epsilon}_1$ the Rabi frequency of the microwave transition to the bound state is proportional to

$$D_{\rm RF} = |\langle\psi_p|\hat{\boldsymbol{d}}_{\rm 2atom} \cdot \vec{\boldsymbol{\epsilon}}_1|\psi_i\rangle|, \tag{7}$$

where

$$\hat{\boldsymbol{d}}_{\rm 2atom} = \hat{\boldsymbol{d}}^{(1)} + \hat{\boldsymbol{d}}^{(2)}. \tag{8}$$

The dependence of $D_{\rm RF}$ on the interatomic separation R for $\theta = 0$ is shown in Fig. 5(b). Since $D_{\rm RF}$ is large at the position of the potential minimum where the Franck-Condon factor associated with the transition $|\psi_i\rangle \to |\psi_p\rangle$ is maximal, the molecular dimer state can be excited efficiently via microwave radiation.

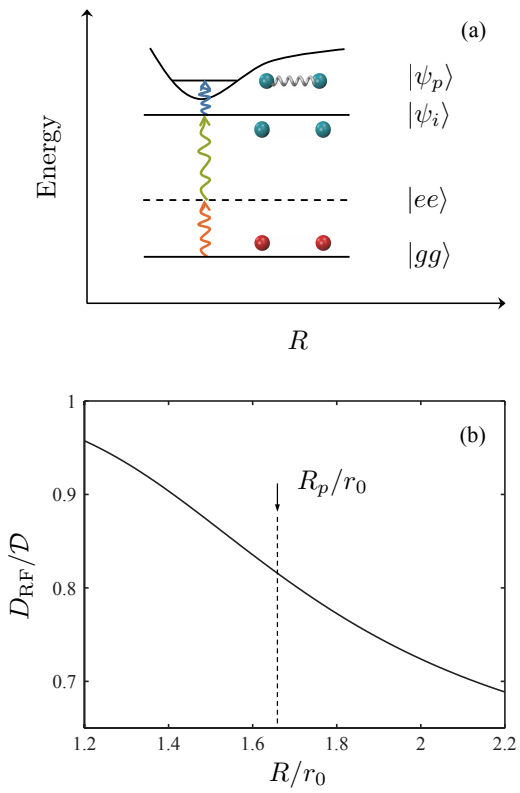

FIG. 5. (Color online) (a) Schematic illustration of the excitation scheme. A two-photon transition couples the ground state $|gg\rangle$ to a two-atom Rydberg state $|\psi_i\rangle$ via an intermediate state $|ee\rangle$. The atoms are excited by microwave fields from the $|\psi_i\rangle$ to a bound state $|\psi_p\rangle$. (b) Transition dipole matrix element between a particular bound state $|\psi_p\rangle$ [see text for details] and the initial state $|\psi_i\rangle$ in Eq. (6) for σ^- polarized light. The parameters are $\Delta/\delta = 100$, $\theta = 0$ and $\mathcal{D}$ is defined in Eq. (A9).

The extreme sensitivity of Rydberg atoms to external electric fields can be used for state selectively ionizing the atoms and then detecting the resulting electrons and ions with high efficiency. Specifically, the bound state $|\psi_p\rangle$ can be experimentally observed by first exciting it to a higher-lying $nsn'd$ state, and then detecting the $n'd$ atom via state-selective field ionization [34–36].

III. THREE-ATOM BOUND STATES

Next we consider three DD interacting Rydberg atoms placed in an external electric field $\boldsymbol{E}$, see Fig. 6(a). This setup was introduced in [29], where it was found that the DD interaction can give rise to three-body bound states. These trimer states represent a genuine three-particle ef-

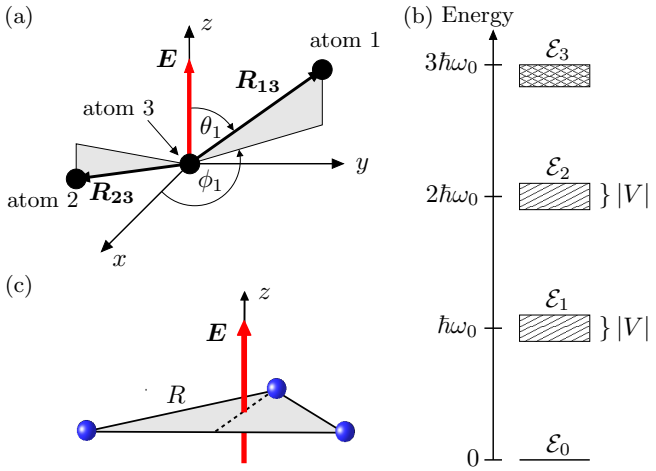

FIG. 6. (Color online) (a) System configuration of three DD interacting Rydberg atoms in an external electric field $\boldsymbol{E}$. The relative position vectors $\boldsymbol{R}_{\alpha 3}$ ($\alpha \in \{1,2\}$) are expressed in terms of spherical coordinates $R_{\alpha 3}$, θ_α and ϕ_α. The angles θ_1 and ϕ_1 are indicated in the figure, while θ_2 and ϕ_2 were omitted in order to keep the drawing concise. (b) Level structure of the three-atom state space. $\mathcal{E}_i$ contains all states where i atoms are in an np state and all other in an ns state. States within $\mathcal{E}_1$ and $\mathcal{E}_2$ are coupled by the DD interaction. (c) Geometry where the atoms form the vertices of an equilateral triangle with edge length R in the $x-y$ plane. The z direction is distinguished by the external electric field $\boldsymbol{E}$.

fect because they cannot be explained by a pairwise binding of the atoms. They arise from a variation of the mechanism described in Sec. II B where the fine structure splitting is replaced by Stark shifts between Zeeman states. This binding mechanism was shown in [29] to be fundamentally different from the Efimov systems in [37–39], where a resonant two-body interaction can be described by a single scattering length exceeding all physically relevant length scales [40, 41].

The aim of this section is to investigate DD induced trimer states in the system shown in Fig. 6(a) and for the level scheme in Fig. 1(b). This extends the original study in [29] where only the $ns_{1/2}$ and $np_{3/2}$ multiplets were considered. In Sec. III A, we briefly describe the system and divide the state space of the three atoms in subspaces in order to facilitate the analysis. We find that the general mechanism for the formation of bound states described in Sec. II B gives rise to more deeply bound trimer states as compared to the states in [29] [see Sec. III B]. Furthermore, we investigate the influence of the $np_{1/2}$ states on the trimer states reported in [29]. In Sec. III C we discuss in detail one trimer state in the $nsnsnp$ manifold which only arises if the $np_{1/2}$ states are taken into account. The latter state has a direct transition dipole moment with states in the $nsnsns$ manifold which facilitates its preparation.

A. The system

The internal states of the three-atom system in Fig. 6(a) are determined by the Hamiltonian

$$H_{\rm int} = \sum_{\alpha=1}^{3} H_{\rm A}^{(\alpha)} + V_{13}(\hat{\boldsymbol{R}}_{13}) + V_{23}(\hat{\boldsymbol{R}}_{23}) + V_{12}(\hat{\boldsymbol{R}}_{12}). \tag{9}$$

Note that all DD interactions between the three atoms described by $H_{\rm int}$ are pairwise interactions. Next we briefly recall some of the notation introduced in [29]. First, we express the two relative position vectors $\boldsymbol{R}_{\alpha 3}$ ($\alpha \in \{1,2\}$) in terms of spherical coordinates,

$$\boldsymbol{R}_{\alpha 3} = R_{\alpha 3}(\sin\theta_\alpha \cos\phi_\alpha, \sin\theta_\alpha \sin\phi_\alpha, \cos\theta_\alpha). \tag{10}$$

It follows that the Born-Oppenheimer surfaces of the Hamiltonian in Eq. (9) can be characterized in terms of the five independent variables

$$\boldsymbol{v} = (R_{13}, R_{23}, \theta_1, \theta_2, \phi), \tag{11}$$

where $\phi = \phi_1 - \phi_2$. Note that ϕ_1 and ϕ_2 are not independent variables because the azimuthal symmetry of the system makes the energies independent of $\phi_1 + \phi_2$. Second, the three-atom states of the system can be conveniently grouped in four subspaces $\mathcal{E}_i$ ($i \in \{0,1,2,3\}$), where $\mathcal{E}_i$ contains all three-atom states with i atoms in an np state and $3-i$ atoms in an ns state. States in $\mathcal{E}_i$ are clustered in energy around $i \times \hbar\omega_0$ as shown in Fig. 6(b). Due to their large energy separation we neglect any DD induced coupling between them and diagonalize H in Eq. (9) in each subspace $\mathcal{E}_i$ independently. We have verified numerically that this is an excellent approximation for the parameter regime considered in the remaining part of this section. Finally, we recall that the Hamiltonian in Eq. (9) is time-reversal invariant [29, 42] and gives rise to Kramers degeneracy. Every eigenvalue of $H_{\rm int}$ in Eq. (9) is thus (at least) two-fold degenerate. In the following Secs. III B and III C we investigate the level structure of the subspaces $\mathcal{E}_1$ and $\mathcal{E}_2$ and the trimer states within them.

B. Potential surfaces in $\mathcal{E}_2$

We consider the geometrical setup shown in Fig. 6(c) and investigate three-body bound states in the subspace $\mathcal{E}_2$. All potential curves in $\mathcal{E}_2$ are shown in Fig. 7(a) as a function of the triangle edge length R. There are three different independent atom asymptotes at energies 0, $\hbar\Delta$ and $2\hbar\Delta$ for large values of R, corresponding to the $nsnp_{3/2}np_{3/2}$, $nsnp_{3/2}np_{1/2}$ and $nsnp_{1/2}np_{1/2}$ manifolds, respectively. Several avoided crossings between potential curves are visible in Fig. 7(a), giving rise to potential wells according to the mechanism explained in Sec. II B. Two wells are highlighted by the green dashed

lines in Fig. 7(a) as an example. The minima occur in a region between r_0 and $1.7r_0$ and are also present without an electric field and the associated Stark shift δ between Zeeman sublevels in the $np_{3/2}$ manifold. We find that the influence of the Stark shift δ is negligible on the energy scale set by the fine structure splitting Δ and for the parameters chosen in Fig. 7(a).

Next we investigate the influence of the $np_{1/2}$ states on the trimer states reported in [29]. In the latter system the depth of the potential wells are of the order of the Stark splitting $|\delta|$ which is typically much smaller than the fine structure interval $\hbar|\Delta|$. Figure 7(b) shows a magnified view of some of the potential curves in Fig. 7(a) and on an energy scale that is comparable to $\hbar|\delta|$. A lot of the potential curves in Fig. 7(b) have local minima, and the trimer potentials investigated in [29] are represented by the red solid and blue dashed curves. The corresponding potential curves for the reduced level scheme considered in [29] are shown in Fig. 7(c). A comparison of Figs. 7(b) and (c) shows that the $np_{1/2}$ states shift the minima of the potential curves towards larger values. The equilibrium value of R for the red solid (blue dashed) curve in Fig. 7(b) is 1.22 (1.06) times larger than for the case without $np_{1/2}$ states in Fig. 7(c). In addition, the presence of the $np_{1/2}$ states compresses the potential curves leading to larger oscillation frequencies describing the quantum dynamics in the wells [29]. For the red solid curve in Fig. 7(b) those frequencies are about 10% larger as compared to the the case without $np_{1/2}$ states. Note that the parameters in Figs. 7(b) and (c) correspond to $\Delta/\delta = 100$. We find that the impact of the $np_{1/2}$ states on the trimer states reported in [29] reduces for larger values of Δ/δ.

The potential wells indicated by the red solid and blue dashed lines in Fig. 7(b) are induced by the Stark shift δ. On the contrary, there are additional and deeper wells in Fig. 7(b) that exist even without an external electric field. Since these wells are absent in Fig. 7(c), they are a consequence of avoided crossings with potential curves from the $np_{1/2}$ manifold. Their physical origin is thus related to the potential wells shown in Fig. 7(a).

So far we analyzed only minima in the potential curves as a function of the triangle edge length R. As discussed above the potential minima in Fig. 7(a) exist even for $\delta = 0$ where the system is spherically symmetric. Three-body bound states for $\delta = 0$ will thus be invariant under uniform rotations of the relative position vectors R_{13} and R_{23}, which is in contrast to the system described in [29]. A more detailed analysis of the angular dependence of trimer states are presented in the next section III C where we investigate potential curves in the manifold $\mathcal{E}_1$. In contrast to the states in $\mathcal{E}_2$, states in $\mathcal{E}_1$ can have a direct transition dipole moment with states in $\mathcal{E}_0$ such that they do not need to be excited via a two-photon process.

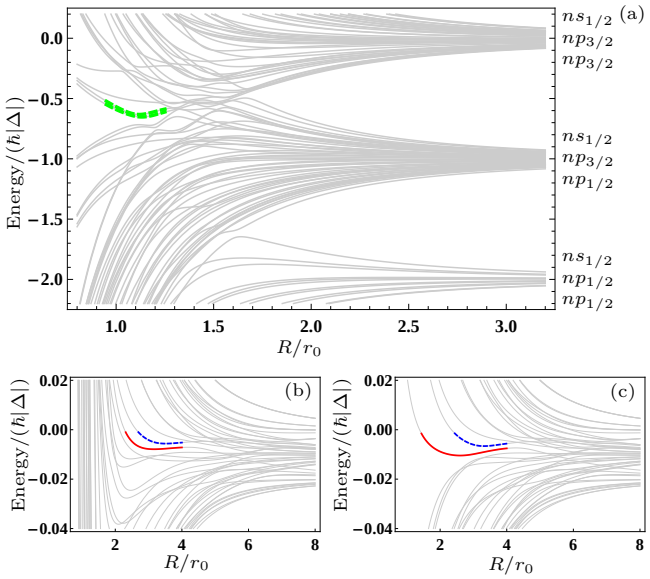

FIG. 7. (Color online) (a) Potential curves within the manifold $\mathcal{E}_2$ for $\Delta/\delta = 100$. (b) Magnified view of potential curves converging to the $ns_{1/2}np_{3/2}np_{3/2}$ asymptote. Note the change in energy and length scales as compared to (a). The red solid and blue dashed curves correspond to the trimer configurations discussed in [29]. (c) Same as in (b), but without the $p_{1/2}$ states as in [29].

C. Potential surfaces in $\mathcal{E}_1$

In this section we investigate the potential curves in the $\mathcal{E}_1$ manifold for the geometrical setup shown in Fig. 6(c). All potential curves in $\mathcal{E}_1$ are shown in Fig. 8(a) as a function of the triangle edge length R. The red solid curve labels the potential well ϵ_p which has a local minimum at $R_p = 1.66r_0$. This minimum corresponds to the parameters $\boldsymbol{v}_p = (R_p, R_p, \pi/2, \pi/2, \pi/3)$. In order to establish that the potential curve ϵ_p has a true minimum with respect to all independent variables we follow the approach outlined in [29]. We find that the gradient of ϵ_p with respect to the independent variables $\boldsymbol{v}$ vanishes at $\boldsymbol{v}_p$, and the Hessian matrix of ϵ_p is positive definite. This shows that ϵ_p has indeed a local minimum at $\boldsymbol{v}_p$. This result holds only in the presence of the external field since the system becomes isotropic for $\delta = 0$. Note that the equilibrium distance R_p between the atoms in the trimer configuration coincides with the atomic separation in the dimer state discussed in Sec. II C 1. Despite this result the stability of the trimer configuration in the subspace $\mathcal{E}_1$ cannot be fully explained by the pairwise binding energies of the atoms. This would only be the case if the trimers were in a product state. On the contrary, the reduced quantum state of two atoms obtained by tracing out one atom is a mixed state and hence the trimer state is entangled. Moreover, some components of the reduced two-atom state reside in the $nsns$ subspace where the atoms are unbound.

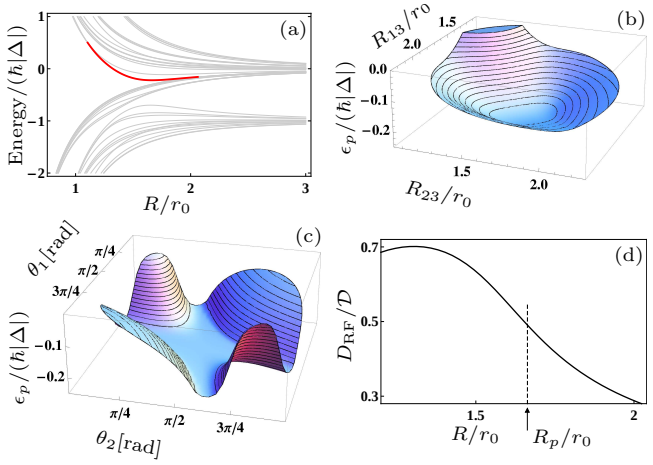

FIG. 8. (Color online) (a) All potential curves within the manifold $\mathcal{E}_1$. The red solid curve shows ϵ_p. (b) Variation of the energy surface ϵ_p with R_{13} and R_{23} for $\theta_1 = \theta_2 = \pi/2$, $\phi = \pi/3$ and $\Delta/\delta = 100$. (c) Dependence of ϵ_p on θ_1 and θ_2 for $R_{13} = R_{23} = R_{\rm min}$, $\phi = \pi/3$ and $\Delta/\delta = 100$. (d) Transition dipole matrix element between the bound state $|\psi_p\rangle$ and the ground state $|\psi_i\rangle$ in Eq. (13) as a function of the triangle edge length R.

The dependence of ϵ_p on the parameters $\boldsymbol{v}$ around the minimum at $\boldsymbol{v}_p$ is shown in Figs. 8(b) and (c). The potential curve ϵ_p has a deep minimum if R_{13} and R_{23} are varied and the remaining parameters are fixed at $\theta_1 = \theta_2 = \pi/2$ and $\phi = \pi/3$ [see Fig. 8(b)]. The depth of the potential well is approximately given by $0.1\hbar|\Delta|$ corresponding to trapping frequencies of the order of 100 MHz for $n \approx 40$. The potential surface in Fig. 8(c) shows ϵ_p as a function of θ_1 and θ_2 for $R_{13} = R_{23} = R_p$ and $\phi = \pi/3$. The four deep valleys in the energy landscape correspond to parameters that are energetically equivalent to the initial configuration $\boldsymbol{v}_p$ in the absence of the electric field. The small Stark shift δ breaks the spherical symmetry of the system and results in a weak trapping of the trimer in the plane perpendicular to the electric field.

1. *Quantum dynamics*

Next we discuss the quantum dynamics of the three Rydberg atoms in the trimer potential ϵ_p as described in detail in [29]. The frequencies of the normal modes of the trimer configuration are given by

$$\omega_1 = 1.04 \times \omega_{\rm vib}, \qquad \omega_2 = \omega_3 = 0.31 \times \omega_{\rm vib},$$
$$\omega_4 = \omega_5 = 0.03 \times \omega_{\rm vib}, \tag{12}$$

where $\omega_{\rm vib}$ is defined in Eq. (5). The frequency ω_1 belongs to the symmetric stretch mode, and the degenerate frequencies ω_2 and ω_3 correspond to the scissor and asymmetric stretch modes, respectively. The two frequencies ω_4 and ω_5 are equal and describe wagging and twisting, respectively. These frequencies are roughly an order of magnitude smaller than the other frequencies because they are only different from zero in the presence of the (small) Stark shift δ. Each of the three Rydberg atoms constituting the trimer state is in a coherent superposition of ns and np states. The radiative lifetime of each atom can be calculated from the lifetimes of the $ns_{1/2}$ $np_{1/2}$ and $np_{3/2}$ Rydberg states [33]. For Rb atoms with $n = 60$ we find that the decay rate at a temperature of 300 K is approximately 9 kHz, which is much smaller than the largest oscillation frequency $\omega_1 = 210$ kHz. The equilibrium edge length of the trimer state for these parameters is $R_p \approx 4.0\,\mu$m which can be experimentally resolved [30, 31].

2. *Preparation*

The efficient excitation of the trimer state $|\psi_p\rangle$ from a state $|\psi_i\rangle$ in the subspace $\mathcal{E}_0$ via microwave fields requires a non-zero transition dipole matrix element between them. Here we assume that the atoms are initially prepared in the state

$$|\psi_i\rangle = |s_{1/2}, -1/2, s_{1/2} - 1/2, s_{1/2} - 1/2\rangle \tag{13}$$

and consider π polarized microwave fields. For the geometry under consideration we find that polarization directions perpendicular to $\boldsymbol{e}_z$ do not couple $|\psi_i\rangle$ and $|\psi_p\rangle$. The excitation Rabi frequency is directly proportional to the dipole matrix element

$$D_{\rm RF} = |\langle\psi_p|\hat{\mathbf{d}}_{\rm 3atom} \cdot \hat{\boldsymbol{e}}_z|\psi_i\rangle|, \tag{14}$$

where

$$\hat{\boldsymbol{d}}_{\rm 3atom} = \hat{\boldsymbol{d}}^{(1)} + \hat{\boldsymbol{d}}^{(2)} + \hat{\boldsymbol{d}}^{(3)}. \tag{15}$$

The value of $D_{\rm RF}$ as a function of the triangle edge length is shown in Fig. 8(d). Note that we chose the state $|\psi_p\rangle$ in the two-dimensional subspace induced by Kramers degeneracy which maximizes $D_{\rm RF}$. Since $D_{\rm RF}$ is large at the position of the potential minimum where the Franck-Condon factor associated with the transition $|\psi_i\rangle \to |\psi_p\rangle$ is maximal, efficient excitation of the trimer state via microwave radiation is possible.

IV. CONCLUSION

In this paper we show that the DD interaction between two and three Rydberg atoms with non-overlapping electron clouds can give rise to bound states. We focus on two different types of dimer and trimer states. The first one arises from avoided crossings between Stark-shifted Rydberg levels that are resonantly coupled by the DD interaction. These states were discussed previously in

two-atom [28] and three-atom [29] systems in a simplified level scheme ignoring the $np_{1/2}$ states in Fig. 1(a). Here we show that the inclusion of the $np_{1/2}$ states leaves the qualitative feature of the dimer (trimer) states investigated in [28] ([29]) unchanged. We provide quantitative corrections for the position and oscillation frequencies of the trimer states discussed in [29]. The second type of bound states arises from avoided crossings between Rydberg states that are separated by the energy difference between the $np_{3/2}$ and $np_{1/2}$ manifolds in the limit of large atomic separations. These dimer and trimer states have not been reported previously and do not require an external electric field. The depth of the potential wells and typical oscillation frequencies describing the quantum dynamics are enhanced by at least one order of magnitude as compared to the states investigated in [28, 29]. We show that the novel dimer and trimer states can be efficiently excited via microwave fields. Typical equilibrium distances of the atoms in the bound states are of the order of several microns, and atoms can be prepared and detected in geometries at those length scales [9, 30, 31]. We find that electric fields can be employed to align the molecules. The dimer configuration can be aligned along the electric field axis and the trimer configuration can be trapped in a plane perpendicular to this axis. In conclusion, we are confident that the dimer and trimer states can be produced and detected with existing technology.

ACKNOWLEDGMENTS

The authors acknowledge financial support from the National Research Foundation and the Ministry of Education, Singapore.

Appendix A: Atomic Hamiltonian and DD Interaction

The atomic Hamiltonian $H_{\rm A}^{(\alpha)}$ of atom α and with the level scheme depicted in Fig. 1(a) is given by

$$\begin{aligned} H_{\rm A}^{(\alpha)} = \hbar[&\omega_0|p_{3/2}-3/2\rangle_\alpha\langle p_{3/2}-3/2|_\alpha \\ &+\omega_0|p_{3/2}+3/2\rangle_\alpha\langle p_{3/2}+3/2|_\alpha \\ &+(\omega_0+\delta)|p_{3/2}-1/2\rangle_\alpha\langle p_{3/2}-1/2|_\alpha \\ &+(\omega_0+\delta)|p_{3/2}+1/2\rangle_\alpha\langle p_{3/2}+1/2|_\alpha \\ &+(\omega_0+\Delta)|p_{1/2}-1/2\rangle_\alpha\langle p_{1/2}-1/2|_\alpha \\ &+(\omega_0+\Delta)|p_{1/2}+1/2\rangle_\alpha\langle p_{1/2}+1/2|_\alpha], \end{aligned} \quad \text{(A1)}$$

where ω_0 is the resonance frequency of the $|ns_{1/2}\rangle \leftrightarrow |np_{3/2}\rangle$ transition.

The DD interaction [43] between atoms α and β located at positions $\boldsymbol{R}_\alpha$ and $\boldsymbol{R}_\beta$ is defined as

$$V_{\alpha\beta}(\boldsymbol{R}) = \frac{1}{4\pi\varepsilon_0 R^3}[\hat{\boldsymbol{d}}^{(\alpha)}\cdot\hat{\boldsymbol{d}}^{(\beta)} - 3(\hat{\boldsymbol{d}}^{(\alpha)}\cdot\vec{\boldsymbol{R}})(\hat{\boldsymbol{d}}^{(\beta)}\cdot\vec{\boldsymbol{R}})], \quad \text{(A2)}$$

where $\hat{\boldsymbol{d}}^{(\alpha)}$ is the electric dipole-moment operator of atom α, $\boldsymbol{R} = \boldsymbol{R}_\alpha - \boldsymbol{R}_\beta$ and $\vec{\boldsymbol{R}} = \boldsymbol{R}/R$ is the corresponding unit vector. Matrix elements of the electric-dipole-moment operator $\hat{\boldsymbol{d}}$ of an individual atom are evaluated via the Wigner-Eckert theorem [44, 45],

$$\begin{aligned} <n'l'_{j'}m'|\hat{d}_q|nl_jm> = (-1)^{\rm j+l'-1/2} &C^{j'm'}_{jm1q}\sqrt{2j+1} \\ &\times \left\{ \begin{array}{ccc} l & 1/2 & j \\ j' & 1 & l' \end{array} \right\} <n'l' \parallel \hat{\boldsymbol{d}} \parallel nl>, \end{aligned} \quad \text{(A3)}$$

where $\hat{d}_q$ ($q \in \{-1,0,1\}$) are the spherical components of the dipole operator,

$$\hat{d}_1 = -\frac{\hat{d}_x + i\hat{d}_y}{\sqrt{2}}, \quad \hat{d}_0 = \hat{d}_z, \quad \hat{d}_{-1} = \frac{\hat{d}_x - i\hat{d}_y}{\sqrt{2}}, \quad \text{(A4)}$$

$C^{j'm'}_{jm1q}$ are Clebsch-Gordan coefficients, and the 3×2 matrices in curly braces are Wigner $6-j$ symbols. The reduced dipole matrix element in Eq. (A3) can be written as [44, 45]

$$<n'l' \parallel \hat{\boldsymbol{d}} \parallel nl> = \sqrt{2l+1}C^{l'0}_{l010}e\langle n'l'|r|nl\rangle, \quad \text{(A5)}$$

where e is the elementary charge and $\langle n'l'|r|nl\rangle$ is a radial matrix element. Combining Eqs. (A3) and (A5) for $n' = n$, $j = 1/2$, $l' = p$ and $l = s$, we obtain

$$\langle np_{3/2}m'|\hat{\boldsymbol{d}}|ns_{1/2}m\rangle = -\mathcal{D}\sum_{q=-1}^{1} C^{3/2m'}_{1/2m1q}\vec{\boldsymbol{\epsilon}}_q, \quad \text{(A6)}$$

$$\langle np_{1/2}m'|\hat{\boldsymbol{d}}|ns_{1/2}m\rangle = \mathcal{D}\sum_{q=-1}^{1} C^{1/2m'}_{1/2m1q}\vec{\boldsymbol{\epsilon}}_q, \quad \text{(A7)}$$

where Eq. (A6) [Eq. (A7)] corresponds to $j' = 3/2$ ($j' = 1/2$). The spherical unit vectors $\vec{\boldsymbol{\epsilon}}_q$ in Eqs. (A6) and (A7) are defined as

$$\vec{\boldsymbol{\epsilon}}_1 = -\frac{\vec{\boldsymbol{x}} - i\vec{\boldsymbol{y}}}{\sqrt{2}}, \quad \vec{\boldsymbol{\epsilon}}_0 = \vec{\boldsymbol{z}}, \quad \vec{\boldsymbol{\epsilon}}_{-1} = \frac{\vec{\boldsymbol{x}} + i\vec{\boldsymbol{y}}}{\sqrt{2}}, \quad \text{(A8)}$$

and

$$\mathcal{D} = \frac{1}{\sqrt{3}}e\langle np|r|ns\rangle \quad \text{(A9)}$$

is a reduced dipole matrix element. For alkali-metal atoms with $n \geq 40$ we have [44] $\langle np|r|ns\rangle \approx n^2 a_0$ where a_0 is the Bohr radius. Since the sums in Eqs. (A6) and (A7) are of the order of unity, the characteristic strength of the DD interaction is given by

$$\hbar\Omega = \frac{|\mathcal{D}|^2}{4\pi\epsilon_0 R^3}. \quad \text{(A10)}$$

The characteristic length scale r_0 in Eq. (3) is obtained by equating Ω in Eq. (A10) with $|\Delta|$.

[1] T. F. Gallagher, *Rydberg Atoms* (Cambridge University Press, Cambridge, 1994)
[2] C. H. Greene, A. S. Dickinson, and H. R. Sadeghpour, Phys. Rev. Lett. **85**, 2458 (2000)
[3] V. Bendkowsky, B. Butscher, J. N. J. P. Shaffer, R. Löw, and T. Pfau, Nature **458**, 1005 (2009)
[4] W. Li, T. Pohl, J. M. Rost, S. T. Rittenhouse, H. R. Sadeghpour, J. Nipper, B. Butscher, J. B. Balewski, V. Bendkowsky, R. Löw, and T. Pfau, Science **334**, 1110 (2011)
[5] J. Tallant, S. T. Rittenhouse, D. Booth, H. R. Sadeghpour, and J. P. Shaffer, Phys. Rev. Lett. **109**, 173202 (2012)
[6] I. C. H. Liu, J. Stanojevic, and J. M. Rost, Phys. Rev. Lett. **102**, 173001 (2009)
[7] J. B. Balewski, A. T. Kruppl, A. Gajl, D. Peter, H. P. Büchler, R. Löw, S. H. T. Pohl, J. M. Rost, S. T. Rittenhouse, H. R. Sadeghpour, J. Nipper, B. Butscher, V. Bendkowsky, and T. Pfau, Nature **502**, 664 (2013)
[8] A. T. Krupp, A. Gaj, J. B. Balewski, P. Ilzhöfer, S. Hofferberth, R. Löw, T. Pfau, M. Kurz, and P. Schmelcher, Phys. Rev. Lett. **112**, 143008 (2014)
[9] L. Béguin, A. Vernier, R. Chicireanu, T. Lahaye, and A. Browaeys, Phys. Rev. Lett. **110**, 263201 (2013)
[10] J. D. Pritchard, K. J. Weatherill, and C. S. Adams, arXiv:1205.4890
[11] M. Saffman, T. G. Walker, and K. Molmer, Rev. Mod. Phys. **82**, 2313 (2010)
[12] D. Jaksch, J. I. Cirac, P. Zoller, S. L. Rolston, R. Côté, and M. D. Lukin, Phys. Rev. Lett. **85**, 2208 (2000)
[13] M. D. Lukin, M. Fleischhauer, R. Côté, L. M. Duan, D. Jaksch, J. I. Cirac, and P. Zoller, Phys. Rev. Lett. **87**, 037901 (2001)
[14] E. Urban, T. A. Johnson, T. Henage, L. Isenhower, D. D. Yavuz, T. G. Walker, and M. Saffman, Nat. Phys. **5**, 110 (2009)
[15] A. Gaëtan, Y. Miroshnychenko, T. W. an A. Chotia, M. Viteau, D. Comparat, P. Pillet, A. Browaeys, and P. Grangier, Nat. Phys. **5**, 115 (2009)
[16] T. Wilk, A. Gaëtan, C. Evellin, J. Wolters, Y. Miroshnychenko, P. Grangier, and A. Browaeys, Phys. Rev. Lett. **104**, 010502 (2010)
[17] L. Isenhower, E. Urban, X. L. Zhang, A. T. Gill, T. Henage, T. A. Johnson, T. G. Walker, and M. Saffman, Phys. Rev. Lett. **104**, 010503 (2010)
[18] B. Zygelman, Phys. Rev. A **86**, 042704 (2012)
[19] M. Kiffner, W. Li, and D. Jaksch, Phys. Rev. Lett. **110**, 170402 (2013)
[20] M. Kiffner, W. Li, and D. Jaksch, J. Phys. B **46**, 134008 (2013)
[21] C. Boisseau, I. Simbotin, and R. Cotè, Phys. Rev. Lett. **88**, 133004 (2002)
[22] A. Schwettmann, J. Crawford, K. R. Overstreet, and J. P. Shaffer, Phys. Rev. A **74**, 020701(R) (2006)
[23] A. Schwettmann, K. R. Overstreet, J. Tallant, and J. P. Shaffer, J. Mod. Opt. **54**, 2551 (2007)
[24] K. R. Overstreet, A. Schwettmann, J. Tallant, D. Booth, and J. P. Shaffer, Nat. Phys. **5**, 581 (2009)
[25] N. Samboy, J. Stanojevic, and R. Côté, Phys. Rev. A **83**, 050501(R) (2011)
[26] N. Samboy and R. Côté, J. Phys. B **44**, 184006 (2011)
[27] N. Samboy and R. Côté, Phys. Rev. A **87**, 032512 (2013)
[28] M. Kiffner, H. Park, W. Li, and T. F. Gallagher, Phys. Rev. A **86**, 031401(R) (2012)
[29] M. Kiffner, W. Li, and D. Jaksch, Phys. Rev. Lett. **111**, 233003 (2013)
[30] P. Schauß, M. Cheneau, M. Endres, T. Fukuhara, S. Hild, A. Omran, T. Pohl, C. Gross, S. Kuhr, and I. Bloch, Nature **491**, 87 (2012)
[31] A. Schwarzkopf, R. E. Sapiro, and G. Raithel, Phys. Rev. Lett. **107**, 103001 (2011)
[32] W. Li, I. Mourachko, M. W. Noel, and T. F. Gallagher, Phys. Rev. A **67**, 052502 (2003)
[33] I. I. Beterov, I. I. Ryabtsev, D. B. Tretyakov, and V. M. Entin, Phys. Rev. A **79**, 052504 (2009)
[34] W. Li, P. J. Tanner, and T. F. Gallagher, Phys. Rev. Lett. **94**, 173001 (2005)
[35] H. Park, P. J. Tanner, B. J. Claessens, E. S. Shuman, and T. F. Gallagher, Phys. Rev. A **84**, 022704 (2011)
[36] H. Park, E. S. Shuman, and T. F. Gallagher, Phys. Rev. A **84**, 052708 (2011)
[37] T. Kraemer, M. Mark, P. Waldburger, J. G. Danzl, C. Chin, B. Engeser, A. D. Lange, K. Pilch, A. Jaakkola, H.-C. Nägerl, and R. Grimm, Nature **440**, 315 (2006)
[38] S. E. Pollack, D. Dries, and R. G. Hulet, Science **326**, 1683 (2009)
[39] Y. Wang, J. P. D'Incao, and C. H. Greene, Phys. Rev. Lett. **106**, 233201 (2011)
[40] V. Efimov, Phys. Lett. B **33**, 563 (1970)
[41] E. Braaten and H.-W. Hammer, Phys. Rep. **428**, 259 (2006)
[42] F. Haake, *Quantum Signatures of Chaos* (Springer, Heidelberg, 2010)
[43] C. Cohen-Tannoudji, J. Dupont-Roc, and G. Grynberg, *Atom-Photon Interactions* (J. Wiley & Sons, 1998)
[44] T. G. Walker and M. Saffman, Phys. Rev. A **77**, 032723 (2008)
[45] A. R. Edmonds, *Angular Momentum in Quantum Mechanics* (Princeton University Press, Princeton, 1960)